SOLIDIFICATION OF A356 ALLOY UNDER DIFFERENT DIRECTIONS AND MAGNITUDES OF STATIC ELECTRICAL FIELD

Sercan Basit
Department of Mechanical Engineering, Faculty of Engineering and Architecture, Kırşehir Ahi Evran University, 40100 Kırşehir, Turkey

Semih Birinci
Department of Metallurgical and Materials Engineering, Graduate School of Natural and Applied Sciences, Yıldız Technical University, 34210 İstanbul, Turkey

Necmettin Maraşlı
Department of Mechanical Engineering, Faculty of Engineering, İstanbul Aydın University, 34294 Sefaköy-Küçükçekmece, İstanbul, Turkey

https://doi.org/10.1007/s40962-021-00641-4

Abstract

A356 alloy, which is a commercial Al–Mg–Si alloy, was solidified with different magnitudes (0.42–1.25 kV cm^{-1}) and directions of static electrical fields (E_+: positive and E_-: negative) to study the influences of E_+ and E_- on irregular interflake structure and mechanical property of Al–Mg–Si alloy. The direction of E is parallel or antiparallel to the solid–liquid (S–L) interface growth direction. The secondary dendrite arm spacing (λ_2), Al_α average grain surface area (S_α), sphericity ratio of Si into matrix (f_{Si}) and Brinell hardness (HB) were measured for A356 alloy solidified with different E_+ and E_- values. The static electrical field force (F) affects the atomic mass flux at the S–L interface during the solidification and thus the microstructure, and physical and mechanical properties of the material are changed with E_+ and E_-. While the values of λ_2, S_α and f_{Si} increase with increasing the value of E_-, the HB value decreases with increasing E_-. However, the values of λ_2, S_α and f_{Si} decrease with increasing the E_+ and the HB value increases with increasing E_+. The relationships between them were determined with linear regression analysis.

Graphic abstract *Optical images of microstructure for the A356 alloy solidified with different directions and magnitudes of static electric fields; (a) 0.0 kV cm^{-1} (b) 1.25 kV cm^{-1} (c) − 1.25 kV cm^{-1}.*

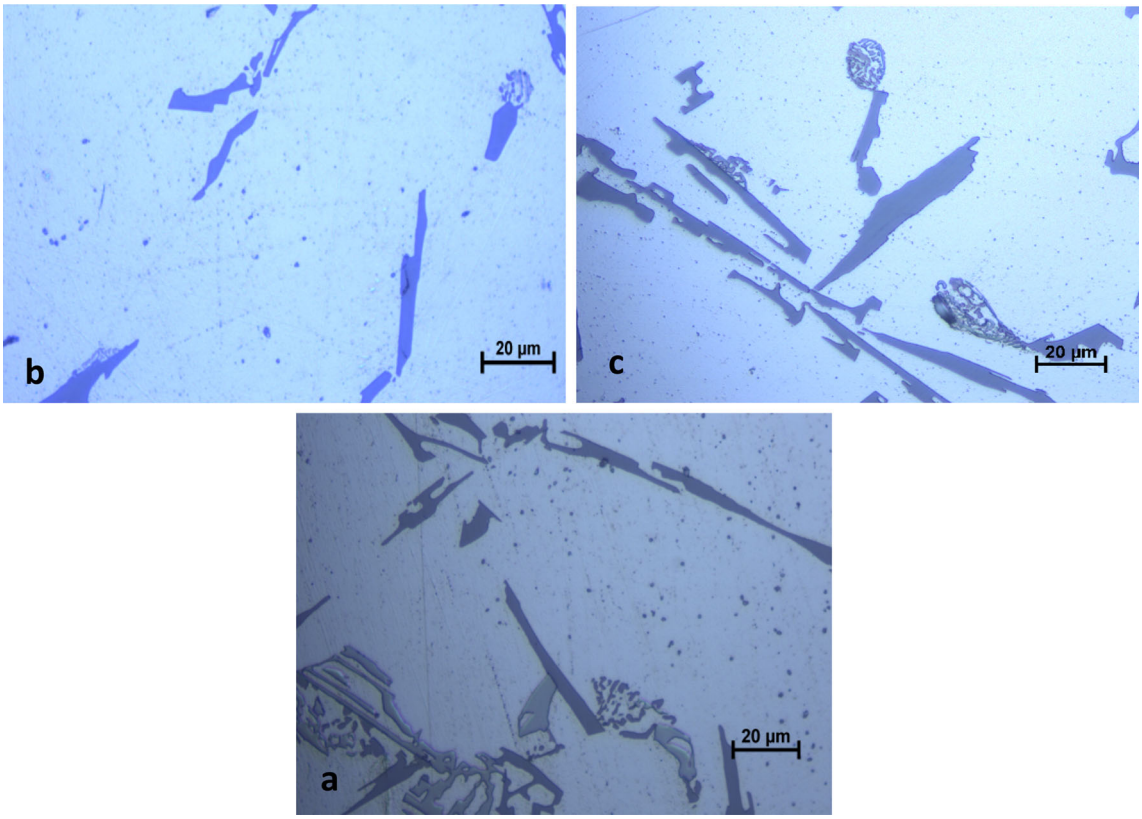

Keywords: *solidification, electric field, A356 alloy, microstructure, hardness, sphericity ratio*

Introduction

It has known that the change in microstructure of metallic materials directly affects its mechanical, physical and corrosion properties. In alloys, the microstructures, the phase dimensions and grain size directly depend on solidification parameters (X, composition of alloy; G, temperature gradient; and V, growth rate). In other words, it is possible to determine the microstructures and hence independently other properties of the alloys by controlling the solidification parameters.

Silicon is the most frequently used alloying element and effectively enhancing both the mechanical properties and castability for the Al-based binary or multicomponent alloys. In particular, the automotive industry has carried out many studies for fuel-based improvements to replace the cast iron alloys with aluminium alloys. For this purpose, the melting conditions, temperature gradient, solidification rate, composition of the alloy and heat treatment that can be applied during and after casting are considered as the main control parameters to obtain the desired microstructure and mechanical properties for aluminium alloys.[1–3] The eutectic silicon modification improves the mechanical properties of the material as well as facilitates casting parts and casting methods[4–5] and the solidification parameters are improved to alter the silicon morphology.

Vibration, compression and semi-solid shaping progresses are commonly preferred to break the secondary dendrite arms and to change the morphology of Si during the solidification in the Al–Si eutectic alloy. The strength property of the material was improved by producing small secondary dendrite arm spacings (λ_2) and changing the morphology of the Si.[2,6–8] The studies also show that the shape factor change for aluminium alloys effects on the microstructure of alloys. Considering these improvements,

it has been concluded that Si affects the mechanical properties of alloys solidified under these conditions.[9]

One way to improve the mechanical properties of Al–Si alloys is to add chemical modifiers that affect the microstructure of the cast components. Small amounts of Sr cause the modification of the eutectic Si particles from a coarse plate-like morphology into a fine fibrous one.[10] The influence of Sr additions on mechanical properties of Al–Si alloys has been extensively investigated.[11–15]

Recently, the researchers have found new external solidification control parameters, which are the semi-solid compaction, agitation, ultrasonic vibration, selective laser melting, alternative current, direct current and DC voltage. They have concluded that the desired mechanical properties of alloys might be obtained by controlling these parameters during the solidification of alloy. In addition to these, there are extra cost effective processes such as grain refinement and heat treatment to improve the mechanical properties of alloys.[16,17]

Alternative current, direct current and magnetic field have been extensively applied into the molten alloys as new alternative external control parameters and their effects on the microstructure and mechanical properties of the alloys were clearly observed.[18–26] In addition, the electrical pulse effects on the distribution of the elements in the electro-pulsing alloy were determined.[20] The molten Bi–Mn eutectic alloy was solidified with the alternating current, static electric field and magnetic field.[21] Manuwong et al.[22] have concluded that the externally applied electro-pulsing is more effective a control parameter than the magnetic flux and Lorentz force parameters in magnetic refinement.

The influences of static external electrical field on microstructure were clearly seen in the Al–Cu eutectic system but the researchers could not fully explain the effect of magnitude and direction of external static electrical field on microstructure.[24] The dependence of microstructure parameter on E_+ and E_- was also not identified and they[24] have just observed that the E_+ and E_- have affected on the lamellar structure and grain sizes.

More recently, Al–33.0 wt.%Cu and Al–6.4 wt.%Ni, which are well-known eutectic systems, were solidified with different magnitudes of E_+ and E_- (7.0–10.0 kV cm^{-1}) to investigate the influences of E_+ and E_- on λ, HB and σ_{UTS} by Basit et al.[25,26] They have observed that lamellar and rod structures, grain sizes and mechanical properties have been significantly influenced by the magnitudes of E_+ and E_- (7.0–10.0 kV cm^{-1}) in the Al–Cu and Al–Ni eutectic systems when its direction is same or opposite with the growth direction of S–L interface.[25,26] According to their investigations, the external high DC voltage applied into molten alloy has occurred a uniform electrical field into molten alloy and thus, the positive and negative static electrical field forces (F_+ and F_-, respectively) have accelerated Al, Cu and Ni atoms at the S–L interface during the solidification. However, the acceleration of Al, Cu and Ni atoms by F_+ and F_- forces is different and the F_+ and F_- forces increase or decrease the atomic mass flux of liquid Al, Cu and Ni atoms at S–L interface, which depend on microstructure and directions of electrical field.

Other well-known commercial Al–Si–Mg alloy (A356), which has dendritic structure, is one of the most widely used aluminium foundry alloys today. Based on the recent work done by Basit et al.[25,26], the influences of E_+ and E_- on irregular interflake microstructure and mechanical properties of A356 alloy are investigated by solidifying the molten A356 alloy under different values of E_+ and E_-. The direction of E is chosen to be parallel or antiparallel to the S–L interface growth direction to see clearly the effects of E_+ and E_- on microstructure and mechanical property of A356 alloy. The present solidification control parameters are kept at same conditions during the solidification under static electrical field and the λ_2, S_α, f_{Si} and HB values for A356 alloy solidified with different E_+ and E_- values are measured with standard measurement techniques.

Materials and Experiments

Experimental Apparatus

An experimental apparatus originally designed by Basit et al.[25,26] was used to solidify the A356 molten alloy with different magnitudes of E_+ and E_- in the present work. The experimental apparatus is schematically represented in Figure 1 and it consists of the preheating furnace, external static electrical field system and cooling tank.

A cylindrical preheating furnace was build-up by winding the Kanthal-A resistance wire on an alumina tube (70 mm ID, 80 mm OD, 100 mm long) to prevent immediately solidification of molten alloy into graphite crucible, prepared in the vacuum melting furnace. The isolated heating zone of preheating furnace was 80 mm in length and the furnace is axially placed on a copper plate electrode (350 mm wide × 350 mm length × 5 mm thick), which is exactly contacted on the cooling tank. The temperature of preheating furnace is kept at least 100 °C above the melting temperature of the alloy.

The external static electrical field system consists of a copper plate electrode (350 mm wide × 350 mm length × 5 mm thick), a vertically adjustable copper disc electrode, which its diameter is greater than the sample diameter and a DC high voltage source, gives 6 kV output with a maximum 30 mA. The space between the disc electrode and plate electrode was 48 mm.

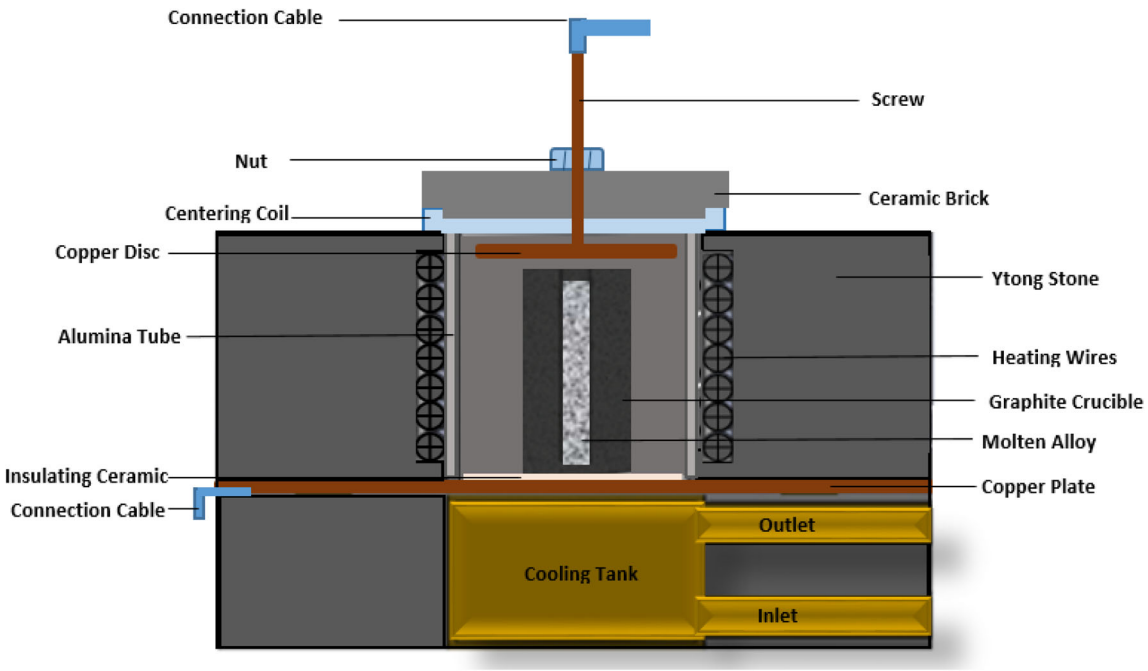

Figure 1. Schematic illustration of experimental apparatus for solidification of alloy under the static electric field.

The cylindrical cooling tank was made of brass to prevent sweating during the cooling. The copper plate electrode was placed on the top of the cooling tank and then the preheating furnace was placed on the copper plate electrode. The water was circulated thought to cooling tank to solidify the molten alloy from the bottom to top of specimen and the temperature of cooling water is kept at 291 K using a heating/refrigerating circulator.

The graphite crucible was directly contacted to the copper plate electrode in previous work. However, the graphite crucible is electrically insulated from the copper plate electrode with a ceramic insulating layer as shown in Figure 1 and the thickness of ceramic layer is about 1 mm in the present work. Thus, the graphite crucible containing the specimen was not used as an electrode and kept into a uniform static electrical field in the present work.

The experimental error in the measurements of the space between the sample and the copper disc is determined as 2.7%.[25]

Solidification of A356 Alloy Under Static Electrical Field

A356 commercial master alloy was supplied from CMS Rim Company. The compositions of A356 according to standard and CMS Rim Company are given in Table 1. The cast A356 alloy was cut into small pieces to melt under vacuum. The sufficient amount of cast A356 alloy was melted into a graphite melting pot (30 mm ID × 40 mm OD and 25 mm in depth with 30 mm total length) under vacuum and the molten A356 alloy was homogenised by mixing with one end closed an alumina tube into a 25 min time interval at least 4 times. The preheating furnace was heated up to 100 K above the alloy melting temperature. After homogenisation of A356 molten alloy, the graphite pot contains molten A356 alloy was quickly removed from the vacuum furnace and then placed into the solidification furnace with the static electrical field.

Table 1. Elemental Analysis of the Commercial Al–Si–Mg (A356) Alloy Used in the Present Work

Elements	Si	Mg	Fe	Ti	Ni	Sr	Al
Wt%	7.31	0.32	0.07	0.11	0.01	0.02	92.16

The static electrical field was utilised into melts by connecting the output terminal of high DC source to copper plate electrode and spacing of 48 mm with the earthed disc electrode or vice versa shown in Figure 2. In addition to protecting the alloy from possible arc and pulse effects, unlike previous studies, the molten alloy was subjected into uniform electric field electrically by insulating it from the electrode. After application of required static electrical field into the molten alloy, the molten A356 alloy was solidified upwards from bottom to top by turning the cooling water on and the input power of preheating furnace off. When the temperature of preheating furnace was fell down 50° below the melting temperature of A356 alloy, the switch of DC voltage supply was turned off and the

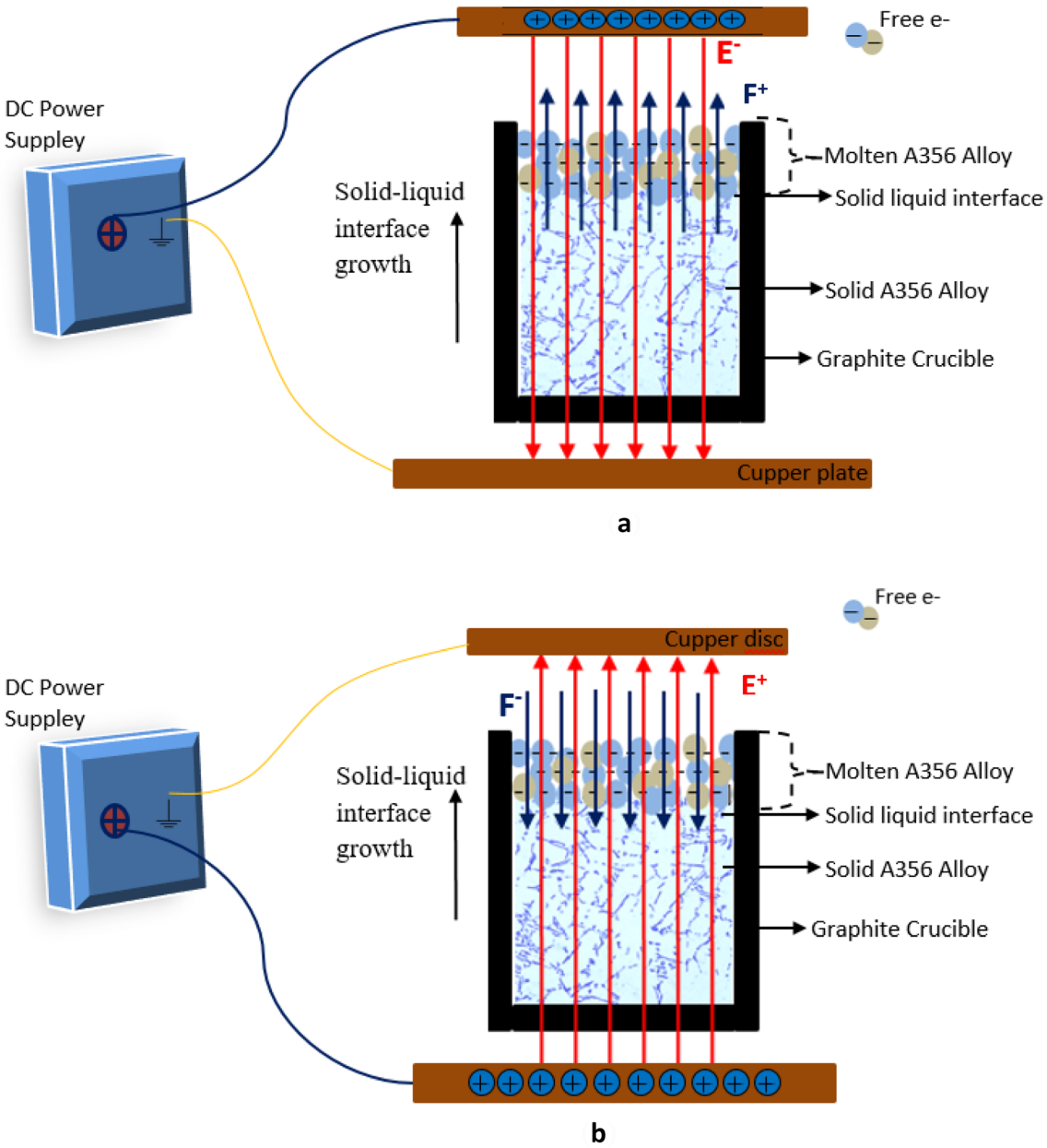

Figure 2. Schematic illustration of dendritic structure growth under the static electrical field at different directions. (a) Negative and (b) positive.

graphite pot was quickly taken out from the solidification furnace. The graphite pot was broken to remove the specimen, and then, the specimen was rapidly quenched by throwing it into the water bath. The solidification process took about 25 min. Solidification experiments for A356 alloy were carried with different E_+ and E_- values (0.412, 0.833 and 1.2 kV cm^{-1}). A reference specimen was also solidified without the electric field under existing solidification conditions.

The total experimental error in the determination of E is found to be 3.0%.[25,26]

Microstructure Observation and Measurements

The dimension of solidified sample was 30 mm in diameter and 25 mm in length. 5 mm thick layer from top of sample was cut out to remove the possible oxide layer and then remain part of sample was cut into two pieces of 10 mm in length. For metallography, the specimens were ground and polished by MiniTech263 polishing machine and then etched with 0.5 wt.% HF agent to display the microstructure for 35–40 s.

The optical images of microstructures for A356 alloy solidified with different values of E_+ and E_- were photographed from cross sections of specimens and the SDAS

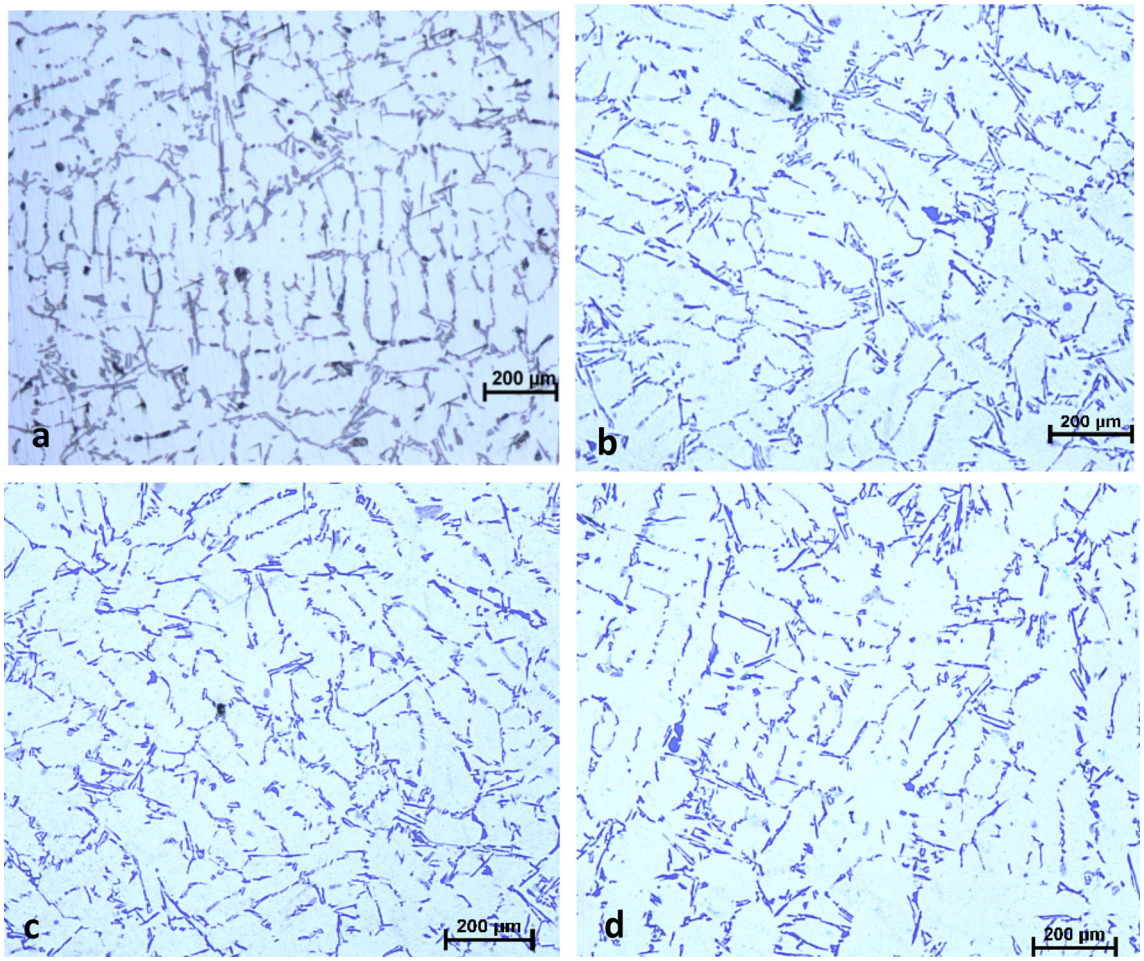

Figure 3. Optical images of dendritic structure for A356 alloy solidified with different magnitudes of E_+. (a) 0.0 kV cm^{-1}, (b) 0.412 kV cm^{-1}, (c) 0.83 kV cm^{-1} and (d) 1.25 kV cm^{-1}.

(λ_2), Al_α grain surface area and sphericity ratio of Si were measured from the optical images using optical microscope's software supplied by Nikon Company. At least 10 measurements for each parameter were taken from inside a central circle with a 20 mm radius for statistical reliability from each sample and then the average value for each parameter was determined.

The statistical error determined with standard division in the measurements of λ_2 is about 10%.[26]

Hardness Measurements

After analysing of microstructures, the cross section surfaces of specimens were again flatted with SiC grinding paper for hardness measurements. The Brinell hardness measurements were taken using a Bulut RBOV-200 type hardness tester, which has 62.5 kg of load with 2.5 mm in diameter a steel ball. At least 10 HB measurements for each sample were taken to get reliable average hardness value. The estimated experiential error in the hardness measurements is 4%.[26]

Results and Discussion

Influences of E_+ and E_- on λ_2, S_α and f_{Si}

The microstructures for A356 alloys solidified with different E_+ and E_- magnitudes are shown in Figures 3 and 4, respectively. As shown in Figures 3 and 4, the microstructure of A356 alloy is composed of a mixture of α-Al dendrites surrounded by Al–Si eutectic phase and the Si particles to form a coarse plate-like morphology, which affects the mechanical properties. It would wonder that whether the Al_α dendrite, irregular Si and intermediate phases could be affected by the applied external static electric fields.

The λ_2 values were measured from optical images taken from the cross sections of samples and the average values of λ_2 with statistical error are given in Table 2. The magnitudes of E_+ and E_- were in the range of 0.42–1.25 kV cm^{-1} in the present work. When the direction of E_- is parallel to the gravity or opposite to the S–L interface growth (solidification) direction, the direction of electric field force acting on liquid metal atoms (F_+) is

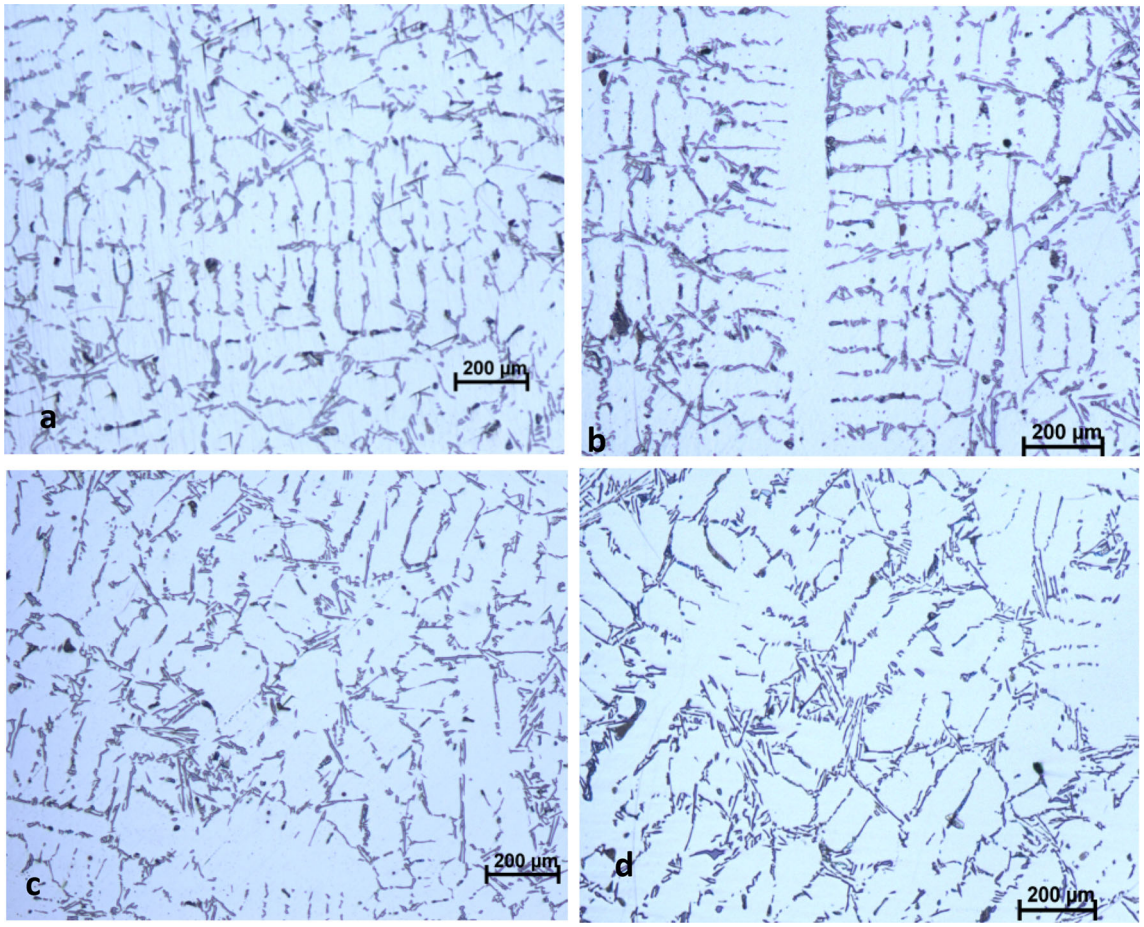

Figure 4. Optical images of dendritic structure for A356 alloy solidified with different magnitudes of E$_-$. (a) 0.0 kV cm^{-1}, (b) − 0.412 kV cm^{-1}, (c) − 0.83 kV cm^{-1} and (d) − 1.25 kV cm^{-1}.

opposite to the direction of E_- or parallel to the S–L interface growth direction and the atomic mass fluxes at S–L interface are decreased with increasing F_+. Thus, the growth rate of S–L interfaces decreases and thus, λ_2 increases with increasing E_- value as shown in Figure 3 and Table 2.

When the direction of applied E_+ is opposite to gravity or parallel to S–L interface growth direction, the direction of electric field force acting on liquid metal atoms (F_-) is opposite to the direction of E_+ or antiparallel to the S–L interface growth direction and the atomic mass fluxes at S–L interface are increased with increasing F_+. Thus, the λ_2 value was decreased by increasing the E_+ value. Thus, the growth rate of S–L interfaces increases and thus, λ_2 decreases with increasing E_+ value as shown in Figure 4 and Table 2.

The increment in the λ_2 is about 10% with the E_- value of 1.25 kV cm^{-1} while the decrement in the λ_2 is about 14% with the E_+ value of 1.25 kV cm^{-1}.

The variations of λ_2 with the E_+ and E_- are plotted in logarithmic scale and given in Figure 5. Figure 5 shows that the variations of λ_2 with E_+ and E_- are linear and the relationships between them were determined from linear regression analysis as

$$\lambda_2^- = 44.90\,\mu\text{m} \times E_-^{0.046} \quad \text{Eqn. 1}$$

$$\lambda_2^+ = 108.64\,\mu\text{m} \times E_+^{-0.049}. \quad \text{Eqn. 2}$$

The regression or correlation coefficients for the λ_2 versus E_+ and E_- plots are 0.9647 and 0.8354, respectively, which are close to 1. It can be seen From Eqs. 1 and 2 that the exponential 0.046 and 0.048 values are close to each other although the coefficient value of 108.64 for E_+ is about twice of the coefficient value of 44.87 for E_-.

Figure 6 shows the variation of the Al$_\alpha$-grain surface area with the E_+ and E_- values for A356 alloy solidified with the different values of E_+ and E_-. As seen from Figure 6 and Table 2, Al$_\alpha$ grain surface area (S_α) increases with increasing the E_-, on the other hand S_α decreases with increasing the E_+. Because of the regression analysis, the dependency of S_α on E_+ and E_- was obtained as:

$$S_\alpha^- = 5038.88\,\mu\text{m}^2 \times E_-^{0.116} \quad \text{Eqn. 3}$$

$$S_\alpha^+ = 60410.58\,\mu\text{m}^2 \times E_+^{-0.118}. \quad \text{Eqn. 4}$$

Table 2. λ_2, S_α, f_{Si} and HB Values for A356 Alloy Solidified with Different Values of E_+ and E_-

	Static electrical field [E (kV cm^{-1})]						
	− 1.250	− 0.833	− 0.412	0.0	0.412	0.833	1.250
Average SDAS, $\lambda_{2,\text{Average}}$ (μm)	76.98 ± 7.70	74.89 ± 7.50	73.11 ± 7.31	70.15 ± 7.01	64.27 ± 6.42	63.31 ± 6.33	60.69 ± 6.06
Al_α grain size (μm^2)	19,794 ± 3958	18,577 ± 3715.4	17,379 ± 3476	17,100 ± 3420	16,817 ± 3363.4	16,472 ± 3294.4	14,589 ± 2917.8
Sphericity ratio of silicon phase (f_{Si})	9,49 ± 2.37	8.36 ± 2.09	7.24 ± 1.81	6.14 ± 1.53	5.96 ± 1.52	5.33 ± 1.35	4,52 ± 1.16
Average Brinell hardness, $HB_{Average}$ (kg mm^{-2})	50,510 ± 2.02	50,940 ± 2.03	56,751 ± 2.27	56,915 ± 2.27	52,143 ± 2.08	55,033 ± 2.20	56,380 ± 2.25

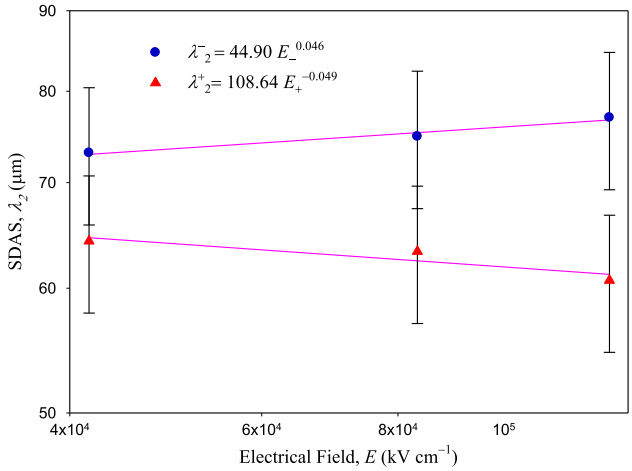

Figure 5. λ_2 versus E_+ and E_- plots for A356 alloy.

The regression coefficients for the S_α versus E_+ and E_- plots are 0.9816 and 0.8372, respectively. From Eqs. 3 and 4, the exponential 0.016 and 0.018 values are also close to each other although the coefficient value of 60,410.5 for E_+ is 11 times of the coefficient value of 44.87 for E_-.

Figure 7 shows the variation of the sphericity ratio of Si (f_{Si}) with the E_+ and E_- for A356 alloy. As discussed above, the S–L interface growth rate decreases, and thus, the increment in the length is higher than the increment of thickness for Si in the case of solidification under E_-. Thus, the sphericity ratio of Si increases with increasing E_-. In the case of solidification under E_+, the S–L interface growth rate increases, and thus, both thickness and length for Si phase decrease. But the decrement in the length is higher than the decrement in the thickness for Si phase under E_+. Thus, the sphericity ratio of Si decreases with increasing E_+. From the regression analysis, the dependency of f_{Si} on the E_+ and E_- is determined as:

$$f_{Si}^- = 0.547 \times E_-^{0.242} \quad \text{Eqn. 5}$$

$$f_{Si}^+ = 79.38 \times E_+^{-0.242}. \quad \text{Eqn. 6}$$

The regression coefficient for the f_{Si} versus E_+ and E_- plots is 0.9871 and 0.9336, respectively, which are close to 1. As can be seen from Eqs. (4) and (5), the exponential values for E_+ and E_- related to sphericity rations are same and thus, the coefficient values of E_- and E_+ should be close to each other. However, the coefficient value of 79.38 for E_+ is about 145 times of the coefficient value of 0.547 for E_- and this disparity is unexpected situation.

The mechanisms of atomic transportations during the solidification can be explained as follows. Metals are conductive materials and have free electrons. To explain present results obtained in the present work for the A356 irregular structure, one assumption is considered that when the electrical fields (E_+ and E_-) are applied into the A356 molten alloy, the electrical fields influenced the liquid

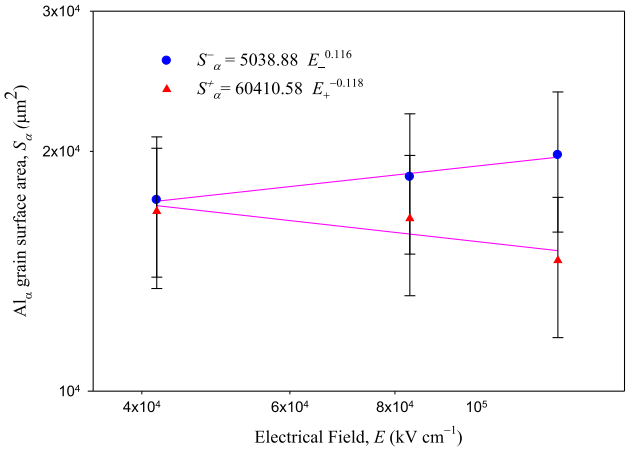

Figure 6. S_α versus E_+ and E_- plots for A356 alloy.

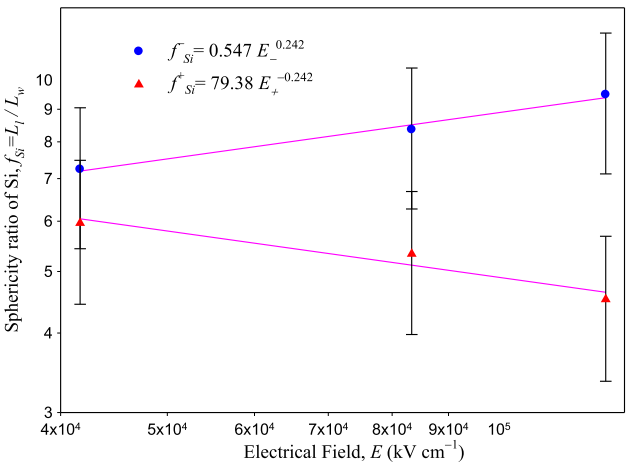

Figure 7. f_{Si} versus E_+ and E_- plots for A356 alloy.

atoms and thus, the electrical field forces (F_- and F_+) affect the liquid metal atoms. From fundamental of physics, the static electric field force acting on i specie liquid atom can accelerate and the acceleration of the i specie atom can be expressed as

$$a_i^E = \frac{F_i}{m_i} = \frac{q_i^* E}{m_i} = \frac{Z_i^* |e| E}{m_i} \qquad \text{Eqn. 7}$$

where m_i is the atomic mass of i specie atom, $F_i = q_i^* E$ is the static electrical field force acting on i specie atom, $q_i^* = Z_i^* |e|$ is the charge of i specie atoms, Z_i^* is the free electron number of metal and $E = \left|\overrightarrow{E}\right|$ is the static electrical field.

The atomic mass transfer of liquid atoms from liquid to solid is therefore affected by F_+ and F_- during the solidification of molten alloy and the electric field forces (F_+ and F_-) will decrease or increase the solidification rate or S–L interface growth rate when the direction of electrical field is parallel or antiparallel to the solidification direction. Thus, the thickness of phases is widened by increasing the value of E_- and got thinner by increasing the value of E_+. Therefore, the mechanical and microstructure of alloy are influenced by E_+ and E_-. The λ_2, S_α and f_{Si} values increase and the HB value decreases with increasing E_-. However, while the S–L interface growth rate is increased by E_+, the λ_2, f_{Si} and S_α values decrease and the HB value increases with increasing E_+.

Dependence of HB on E_+ and E_-

Brinell hardness measurements for A356 alloy solidified with different values of E_+ and E_- were taken on the cross sections of samples, and the average HB values with statistical error are given in Table 2. The variations of HB with E are plotted in Figure 8 and the relationships between them are found as;

$$HB^- = 184.077 \times E_-^{-0.111} \qquad \text{Eqn. 8}$$

$$HB^+ = 24.266 \times E_+^{0.072}. \qquad \text{Eqn. 9}$$

The regression coefficient (r^2) for HB versus E_+ and E_- plots is 0.9079 and 0.9956, respectively, which are close to 1. As shown in Figure 8, the applied external static electric fields into A356 molten alloy seem to clearly influence on the hardness as well as the microstructure. The HB^+ value increases with increasing the value of E_+ while HB^- value decreases with increasing the value of E_-. The exponential 0.111 value of E_- is close to the exponential 0.072 value of E_+ for the A356 alloy and the coefficient 184.077 of E_- is about 87 times of the coefficient 24.266 of E_+. This means that in A356 system, the dependence of HB on the E_+ and E_- is similar but the coefficient disparity is unexpected difference.

A comparison of present results obtained for the A356 alloy solidified with different values of E_+ and E_- with the results obtained for Al-based binary or multicomponent alloys solidified under different solidification conditions[25–30] is given in Table 3. The results obtained in previous works[25–30] are related for the Al-based binary or multicomponent systems at near the eutectic composition

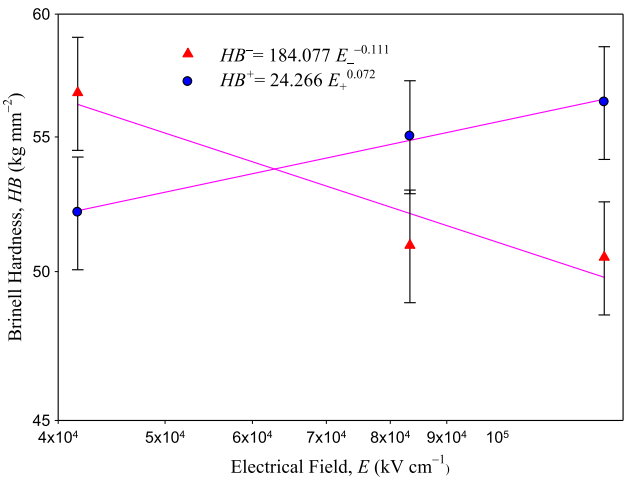

Figure 8. HB versus E_+ and E_- plots for A356 alloy.

Table 3. A Comparison of λ and HB Dependences on E_+ and E_- for A356 Alloy Obtained in the Present Work with λ and HB Dependences on V, E_+ and E_- for Al-Based Binary or Ternary Alloys Obtained in Previous Works

Alloy (wt%)	Solidification parameters			Microstructure Spacings (μm)	Hardness (kg mm^{-2})
	G (K mm^{-1})	V (μm s^{-1})	Static Electrical field (kV cm^{-1})		
Al–12.6Si [Present Study]	–	–	From 0.42 to 1.25	$\lambda_2^+ = 108.64 \times E_+^{-0.049}$	$HB^+ = 91.20 \times {}_+^{-0.16}$
			From 0.42 to 1.25		
				$\lambda_2^- = 44.90 \times {}_-^{0.046}$	$HB^- = 184.077 \times {}_-^{-0.111}$
Al–33.0Cu[25]	–	–	From 8.1 to 10	$\lambda^+ = 1.672 \times {}_+^{2.77}$	$HB^+ = 103.83 \times {}_+^{-0.96}$
			From − 8 to − 10.2		
				$\lambda^- = 0.482 \times {}_-^{-2.00}$	$HB^- = 5.51 \times {}_-^{0.51}$
Al–6.4Ni[26]	–	–	From 8 to 10	$\lambda^+ = 2.57 \times {}_+^{2.87}$	$HB^+ = 2102.03 \times {}_+^{-0.61}$
			From − 7.8 to − 10.2		
				$\lambda^- = 0.73 \times {}_-^{-1.41}$	$HB^- = 0.602 \times {}_-^{0.63}$
Al–12.6Si[27]	7.8	8.3–498.7	–	$\lambda = 23.44 \times^{-0.46}$	–
Al–13Si[28]	7–14	10–2000	–	$\lambda = 55.0 \times^{-0.52}$	–
Al–12.95Si–4.96Mg[29]	9.39	8.64–165.20	–	$\lambda = 29.32 \times^{-0.52}$	$HV = 119.9 \times^{0.07}$
Al–12Si–5Ni–0.4Fe[30]	6.43	8.25–164.81	–	$\lambda = 9.94 \times^{-0.38}$	$HV = 67.9 \times^{0.07}$

and the growth type of S–L interface in that systems are eutectic growth. A356 alloy studied in the present work is off eutectic system and the growth type of S–L interface is dendrite growth. Despite the differences in solidification conditions, compositions and growth types, the present results obtained in the present work seem to be compatible with the results obtained in previous works[25–30].

Conclusions

According to the present results, both the direction and magnitude of E applied into A356 molten alloy have influenced on its microstructure and hardness. Since metallic elements are substances with free electrons, an electric field force affects these electrons if a uniform static electrical field exists into the metallic liquid. The electric field force affects the atomic mass flux and thus the growth rate at the S–L interface is decreased or increased during the solidification. Therefore, the static electrical field influences the microstructure and mechanical and physical properties for metallic alloy when its direction is parallel or antiparallel to the growth direction.

In the experimental studies, as shown in Figure 1, the samples were electrically insulated from the electrodes with an insulating ceramic paint to get a uniform electric field on the specimen. It is this feature that makes this study special that the specimen was not used as one of the electrodes by directly connecting to positive or negative poles of DC voltage supply. The applied electrical field values were in the range 0.42–1.25 kV cm^{-1}. As can be seen from the microstructures shown in Figures 3 and 4, the effects of E on the microstructure could be more clearly seen by applying high E value than the values of 1.25 kV cm^{-1} if it is possible. In the present work, the used DC voltage supply gives maximum 5.5 kV with 40 mA output current, and thus, the voltage application was limited in the present work.

The required voltage values are considered to be appropriate values in terms of providing the necessary precautions to be taken in order to apply the method in the casting industry practically. In order to perform the test experiments at higher voltages, extra safety precautions are needed and the required electrical insulation should be made significantly to protect it from possible arcs and pulses. Although this may seem contrary to the inherent practicality of casting, choosing the directional solidification at unsteady state in the study is for easy application of the innovative approach in foundries. Dependences of microstructure on magnitudes and directions of E are one of the biggest advantages of this study.

Acknowledgements

This work was supported by Yıldız Technical University Scientific Research Project Unit, (FBA-2017-3078). The researchers are thankful to Yıldız Technical University Scientific Research Project Unit for their financial

supports.

REFERENCES

1. S.G. Shabestari, H. Moemeni, Effect of copper and solidification conditions on the microstructure and mechanical properties of Al–Si–Mg alloys. J. Mater. Process. Technol. **153–154**, 193–198 (2004). https://doi.org/10.1016/j.jmatprotec.2004.04.302
2. A.K. Dahle, K. Nogita, S.D. McDonald, C. Dinnis, L. Lu, Eutectic modification and microstructure development in Al–Si alloys. Mater. Sci. Eng. A. **413–414**, 243–248 (2005). https://doi.org/10.1016/j.msea.2005.09.055
3. S.S. Sreeja Kumari, R.M. Pillai, T.P.D. Rajan, B.C. Pai, Effects of individual and combined additions of Be, Mn, Ca and Sr on the solidification behaviour, structure and mechanical properties of Al–7Si–0.3Mg–0.8Fe alloy. Mater. Sci. Eng. A. **460–461**, 561–573 (2007). https://doi.org/10.1016/j.msea.2007.01.082
4. J.E. Gruzleski, B.M. Closset, *The Treatment of Liquid Aluminum-Silicon Alloys* (Am. Foundrymen's Soc, USA, 1990)
5. C. Brian, K. O'Reilly, *Solidification and Casting* (Institute of Physics Publishing Bristol and Philadelphia, United Kingdom, 2003)
6. R. Li, L. Liu, L. Zhang, J. Sun, Y. Shi, B. Yu, Effect of squeeze casting on microstructure and mechanical properties of hypereutectic Al–*x*Si alloys. J. Mater. Sci. Technol. **33**, 404–410 (2017). https://doi.org/10.1016/j.jmst.2017.02.004
7. A. Kisasoz, K.A. Guler, A. Karaaslan, Influence of orbital shaking on microstructure and mechanical properties of A380 aluminium alloy produced by lost foam casting. Russ. J. Non-Ferrous Met. **58**, 238–243 (2017). https://doi.org/10.3103/S1067821217030063
8. H.K. Jung, C.G. Kang, Induction heating process of an Al–Si aluminum alloy for semi-solid die casting and its resulting microstructure. J. Mater. Process. Technol. **120**, 355–364 (2002). https://doi.org/10.1016/S0924-0136(01)01162-1
9. Q.D. Qin, Y.G. Zhao, P.J. Cong, W. Zhou, B. Xu, Semisolid microstructure of Mg_2Si/Al composite by cooling slope cast and its evolution during partial remelting process. Mater. Sci. Eng. A. **444**, 99–103 (2007). https://doi.org/10.1016/j.msea.2006.08.074
10. A. Fortini, L. Lattanzi, M. Merlin, G.L. Garagnani, Comprehensive evaluation of modification level assessment in Sr-modified aluminium alloys. Inter Metalcast. **12**, 697–711 (2018). https://doi.org/10.1007/s40962-017-0202-3
11. G. Sigworth, J. Campbell, J. Jorstad, The modification of Al–Si casting alloys: important practical and theoretical aspects. Inter Metalcast **3**, 65–78 (2009). https://doi.org/10.1007/BF03355442
12. S. Hegde, K.N. Prabhu, Modification of eutectic silicon in Al–Si alloys. J. Mater. Sci. **43**, 3009–3027 (2008)
13. G.K. Sigworth, The modification of Al-Si casting alloys: important practical and theoretical aspects. Int. J. Metalcast. **2**, 19–40 (2008)
14. S.G. Shabestari, F. Shahri, Influence of modification, solidification conditions and heat treatment on the microstructure and mechanical properties of A356 aluminium alloy. J. Mater. Sci. **39**, 2023–2032 (2004)
15. G. Eisaabadi, A. Nouri, Effect of Sr on the microstructure of electromagnetically stirred semi-solid hypoeutectic Al–Si alloys. Inter Metalcast. **12**, 292–297 (2018). https://doi.org/10.1007/s40962-017-0161-8
16. E. Sjölander, S. Seifeddine, The heat treatment of Al–Si–Cu–Mg casting alloys. J. Mater. Process. Technol. **210**, 1249–1259 (2010). https://doi.org/10.1016/j.jmatprotec.2010.03.020
17. S. Hegde, K.N. Prabhu, Modification of eutectic silicon in Al–Si alloys. J. Mater. Sci. **43**, 3009–3027 (2008). https://doi.org/10.1007/s10853-008-2505-5
18. H. Conrad, Influence of an electric or magnetic field on the liquid–solid transformation in materials and on the microstructure of the solid. Mater. Sci. Eng. A **287**, 205–212 (2000). https://doi.org/10.1016/S0921-5093(00)00777-2
19. Y. Zhong, J. Wang, T. Zheng, Y. Fautrelle, Z. Ren, Homogeneous hypermonotectic alloy fabricated by electric-magnetic-compound field assisting solidification. Mater. Today Proc. **2**, 364–372 (2015). https://doi.org/10.1016/j.matpr.2015.05.051
20. Z.Y. Liao, H.C. Wang, P. Hong, X. Li, J. Lie, S.J. Wang, G. Wang, M.S. Dargusch, Effect of pulsed electric field on the distribution and migration of P, S, and Si elements of Fe-based alloys. Adv. Mater. Res. **194–196**, 194–196 (2011)
21. Y. Ma, L.L. Zheng, D.J. Larson, Microstructure formation during BiMn/Bi eutectic growth with applied alternating electric fields. J. Cryst. Growth **262**, 620–630 (2004). https://doi.org/10.1016/j.jcrysgro.2003.10.018
22. T. Manuwong, *Solidification of Metal Alloys in Pulse Electromagnetic Fields*. Ph.D Thesis, University of Hull, UK (2015).
23. K.G. Prashanth, S. Scudino, H.J. Klauss, K.B. Surreddi, L. Löber, Z. Wang, A.K. Chaubey, U. Kühn, J. Eckert, Microstructure and mechanical properties of Al–12Si produced by selective laser melting: effect of heat treatment. Mater. Sci. Eng. A. **590**, 153–160 (2014). https://doi.org/10.1016/j.msea.2013.10.023
24. B. Liu, Z. Zhao, Y. Wang, Z. Chen, The solidification of Al–Cu binary eutectic alloy with electric fields. J. Cryst. Growth **271**, 294–301 (2004). https://doi.org/10.1016/j.jcrysgro.2004.06.009

25. S. Basit, S. Birinci, N. Maraşlı, Electro growth of Al–Cu eutectic alloy. Mater. Charact. **161**, 110157 (2020). https://doi.org/10.1016/j.matchar.2020.110157
26. S. Basit, S. Birinci, N. Maraşlı, Growth of rod structure with static electrical field in the Al–Ni eutectic system. J. Mater. Sci. Mater. Electron. **31**, 14055–14068 (2020). https://doi.org/10.1007/s10854-020-03960-0
27. M. Gündüz, H. Kaya, E. Çadirli, A. Özmen, Interflake spacings and undercoolings in Al–Si irregular eutectic alloy. Mater. Sci. Eng. A. **369**, 215–229 (2004). https://doi.org/10.1016/j.msea.2003.11.020
28. S. Steinbach, N. Euskirchen, V. Witusiewicz, L. Sturz, L. Ratke, The influence of fluid flow on intermetallic phases in Al-cast alloys. Mater. Sci. Forum **519–521**, 1795–1800 (2006)
29. N. El Mahallawy, A. Fathy, W. Abdelaziem, M. Hassan, Microstructure evolution and mechanical properties of Al/Al-12%Simultilayer processed by accumulative roll bonding (ARB). Mater. Sci. Eng. A. **647**, 127–135 (2015). https://doi.org/10.1016/j.msea.2015.08.064
30. T. Hosch, R.E. Napolitano, The effect of the flake to fiber transition in silicon morphology on the tensile properties of Al–Si eutectic alloys. Mater. Sci. Eng. A. **528**, 226–232 (2010). https://doi.org/10.1016/j.msea.2010.09.008